J. KSIAM Vol.15, No.3, 223-231, 2011

NUMERICAL APPROACH TO MICROSTRUCTURAL CHARACTERIZATIONS FOR DENSE AND POROUS THERMAL BARRIER COATINGS

SEOKCHAN KIM[1] , JAEGWI GO[2*], YEON-GIL JUNG[2*] AND UNGYU PAIK[3]

[1]DEPARTMENT OF MATHEMATICS, CHANGWON NATIONAL UNIVEISIRY, SOUTH KOREA
E-mail: sckim@changwon.ac.kr

[2]SCHOOL OF NANO AND ADVANCED MATERIALS ENGINEERING, CHANGWON NATIONAL UNIVEISIRY, SOUTH KOREA
E-mail: jggo@changwon.ac.kr and jungyg@changwon.ac.kr

[3]DEPARTMENT OF ENERGY ENGINEERING, HANYANG UNIVERSITY, SOUTH KOREA
E-mail: upaik@hanyang.ac.kr

ABSTRACT. During spray coating, especially in an air plasma spray (APS), pores, cracks, and splat boundaries are developed and those factors exert influence on thermomechanical properties such as elastic modulus, thermal conductivity, and coefficient of thermal expansion. Moreover, the thermo mechanical properties are crucial elements to determine the thermoelastic characteristics, for instance, temperature distribution, displacements, and stresses. Two types of thermal barrier coating (TBC) model, the dense and porous microstructures, are taken into account for the analysis of microstructural characterizations. TriplexPro^{TM}-200 system was applied to prepare TBC samples, and the METECO 204 C-NS powder is adopted for the relatively porous microstructure and METECO 204 NS powder for the dense microstructure in the top coat of TBCs. Governing partial differential equations were derived based on the thermoelastic theory and approximate estimates for the thermoelastic characteristics were obtained using a finite volume method for the governing equations.

1. INTRODUCTION

Thermal barrier coatings (TBCs) are widely employed in hot section components of gas turbines such as combustors and turbine blades to improve their durability. TBC system is composed of three representative layers; a ceramic top coat, a super alloy substrate, and a metallic bond coat between the substrate and the top coat (Fig. 1). Zirconia featuring a low thermal conductivity decreases the substrate temperature, which is concluded in an extension of metal components' lifetime. The microstructure of TBC system is influenced deeply by the feedstock powders and spray condition [5]. The microstructural characterizations of TBC system play important role to determine the thermal and mechanical properties. Especially, the thermal conductivity is very sensitive to the microstructure due to the deposition process [4]. Moreover, the microstructure of TBC system is closely related to the physical phenomena such as wear resistance and failure mechanism, which demands a new desirable coating or process strategies.

Received by the editors May 17, 2011; Revised August 23, 2011; Accepted in revised form September 5, 2011.
2000 *Mathematics Subject Classification.* 93B05.
Key words and phrases. Thermal barrier coating, Plasma spraying, Thermoelasticity
*Corresponding author

Many authors have attempted and investigated the dense vertical cracked TBC, high porosity coatings, and solution precursor plasma spray process methods. The effects of starting powder morphology on the microstructure and mechanical properties of TBCs prepared by an air plasma spray (APS) were studied by Jung *et. al.* [6]. Harris *et. al.* [2] described a new deposition process to create the porous and buffer layers by controlling coating parameter. Cernuschi *et. al.* [1] developed an inversion procedure to evaluate microstructural parameters describing the porosity morphology of porous TBCs from the thermal diffusivity.

In the present research, two types of thermal barrier coating (TBC) model, the dense and porous microstructures, are taken into account for the analysis of microstructural characterizations. TBC samples were prepared using TriplexPro^{TM}-200 system, and the METECO 204 C-NS powder is adopted for the relatively porous microstructure with 20% porosity and METECO 204 NS powder for the dense microstructure with 10% porosity in the top coat of TBCs. Since the microstructure is decisive factor to determine the thermal and mechanical properties, the microstructural characterizations are represented through the thermoelastic behaviors. A couple of partial differential equations is derived based on the thermal elastic theory and a finite volume approach applied for the governing equation to analyze the thermoelastic characteristics. The results and the analysis performed here contribute further understanding to the behaviors of TBCs.

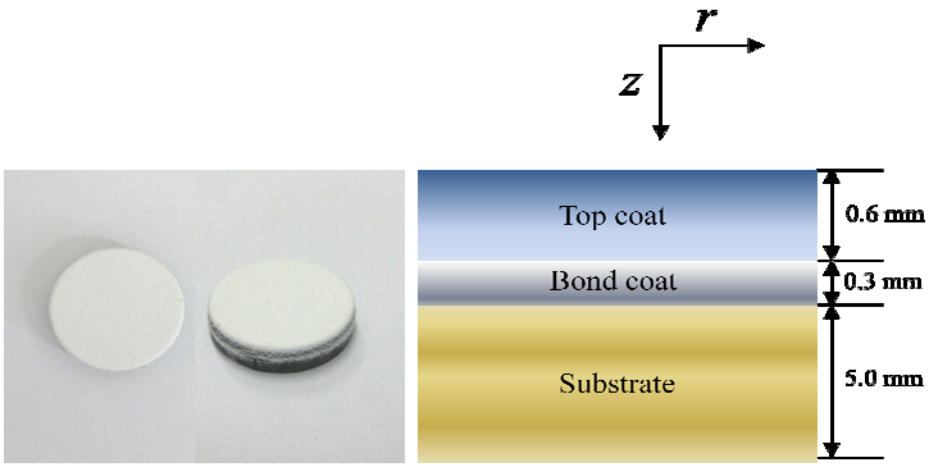

FIGURE 1. A circular disk sample and schematic diagram for thermoelastic characteristics of TBCs

2. MATHEMATICAL MODELLING

2.1. Temperature distribution formulation. The circular disk taken into account is under the action of high temperature and the behaviors of domain are thermoelastic. Temperature distribution profiles thus are necessary for the effects of high temperature to the circular. The differential equation for the circular disk which is subjecting to a uniform temperature loading to the longitudinal z - direction (see Fig. 1) is

$$\frac{\partial^2 T}{\partial z^2} = 0 . \tag{2.1}$$

The general solution of Eq. (2.1) is

$$T(z) = d_1 + d_2 z,$$

where d_1 and d_2 are integral constants. The boundary conditions for differential constants are given by

$$T(z_0) = T_{in},\ T(z_1) = T_1,\quad T(z_2) = T_2,\quad T(z_b) = T_{out}. \tag{2.2}$$

The z_0, z_1, z_2, and z_b represent, respectively, the boundary of the top coat, the interface between the top and bond coats, and the bond coat and the substrate, the boundary of the substrate. But, only two boundary values T_{in} and T_{out} are known, and so additional necessary information are required to obtain a unique temperature distribution profile for each layer. Heat flux at each layer point is considered and the equations for i^{th} layer are expressed as

$$q_i = \frac{k_i}{L_i}(T_{i-1} - T_i),\qquad q_i = q_{i+1}, \tag{2.3}$$

where q_i is the heat flux into i^{th} layer, k_i is the condcutivity and L_i is the length of i^{th} layer. At each i^{th} layer, the integral constants for the temperature distribution profile are determined uniquely by solving the following linear system;

$$\begin{aligned}
&C_{i1} + C_{i2} r_{i-1} = T_{i-1}\\
&C_{i1} + C_{i2} r_i - T_i = 0\\
&q_i = \frac{k_i}{L_i}(T_{i-1} - T_i),\qquad q_i = q_{i+1}\\
&q_{n-1} = \frac{k_{n-1}}{L_{n-1}}(T_{n-2} - T_{n-1}),\qquad q_{n-1} = q_n\\
&q_n - \frac{k_n}{L_n} T_{n-1} = -\frac{k_n}{L_n} T_{out},\qquad i = 1, 2, \cdots, n-1
\end{aligned} \tag{2.4}$$

The T_{i-1} is known value solved by $(i-1)^{th}$ layer linear system and T_{out} is given initial value, and thus the number of $2(n-i)+3$ equations will determine $2(n-i)+3$'s unknown coefficients. Here, n is the number of layer.

2.2. Thermoelastic formulation. According to the assumption that the circular disk is under the action of the longitudinal (z -direction) loading only, all quantities are independent of θ and thus equilibrium equations in polar coordinates can be written by

$$\begin{aligned}
&\frac{\partial \sigma_r}{\partial r} + \frac{\partial \tau_{rz}}{\partial z} + \frac{\sigma_r - \sigma_\theta}{r} = 0\\
&\frac{\partial \tau_{rz}}{\partial r} + \frac{\partial \sigma_z}{\partial z} + \frac{\tau_{rz}}{r} = 0,
\end{aligned} \tag{2.5}$$

where σ_r, σ_θ, τ_{rz}, and σ_z are the radial, circumferential, shear, and longitudinal stress, respectively. Let u be the displacement to the direction r, let v be the displacement to the direction θ, and let w be the displacement to the direction z. Strain-displacement relations

based on the independence of all quantities of θ are the followings;

$$\varepsilon_r = \frac{\partial u}{\partial r}, \qquad \varepsilon_\theta = \frac{u}{r}, \qquad \varepsilon_z = \frac{\partial w}{\partial z}$$

$$\gamma_{r\theta} = 0, \qquad \gamma_{z\theta} = 0, \qquad \gamma_{rz} = \frac{\partial u}{\partial z} + \frac{\partial w}{\partial r}. \tag{2.6}$$

ε_r, ε_θ, ε_z, and γ_{ij} indicate the radial, circumferential, longitudinal strain, and shear strain to the i and j -directions, respectively. The strain-stress relations due to the thermal expansion can be expressed as

$$\varepsilon_r = \frac{1}{E}\left[\sigma_r - \nu(\sigma_\theta + \sigma_z)\right] + \alpha T, \qquad \varepsilon_\theta = \frac{1}{E}\left[\sigma_\theta - \nu(\sigma_r + \sigma_z)\right] + \alpha T$$

$$\varepsilon_z = \frac{1}{E}\left[\sigma_z - \nu(\sigma_r + \sigma_\theta)\right] + \alpha T,$$

$$\tau_{r\theta} = G\gamma_{r\theta} = 0, \qquad \tau_{\theta z} = G\gamma_{\theta z} = 0, \qquad \tau_{rz} = G\gamma_{rz}, \tag{2.7}$$

where $G = 2E(1+\nu)$. E, ν, and α are, respectively, Young's modulus, passion ratio, and CTE. The combination of Eqs. (2.5)-(2.7) leads to the following governing equations;

$$-K(1-\nu)r\frac{\partial}{\partial r}(r\frac{\partial u}{\partial r}) + Gr^2\frac{\partial}{\partial z}(\frac{\partial u}{\partial z}) + K(1-\nu)u = 0 \tag{2.8-a}$$

$$-K(1-\nu)r\frac{\partial}{\partial z}(\frac{\partial w}{\partial z}) + (G - K\nu)\frac{\partial}{\partial r}(\frac{\partial u}{\partial z}) + (\frac{G}{r} - \frac{K\nu}{r})\frac{\partial u}{\partial z} + K\alpha(1+\nu)\frac{\partial T}{\partial z} = 0, \tag{2.8-b}$$

where $K = \dfrac{E}{(1+\nu)(2\nu-1)}$. For the study of thermal elastic behaviors of circular disk samples the following boundary conditions are applied;

$$u(0,z) = 0 \qquad \sigma_r(R,z) = 0 \qquad \sigma_z(r,0) = 0 \qquad \sigma_z(r,z_b) = 0.$$

2.3 Finite volume formulation. A pair of the governing equations is too involved to be solved analytically. A numerical technique thus is required for the approximation and a finite volume method is applied. The domain is divided up into control volume and integrates the field equations over each control volume. The finite surface mesh is denoted by (i, j) and the discretizations for the governing equations are developed based on the following relations at the adjacent locations [3];

$$(\frac{\partial u}{\partial r})_{i,j+\frac{1}{2}} = \frac{u_{i,j+1} - u_{i,j}}{\Delta r}, \qquad (\frac{\partial u}{\partial r})_{i,j-\frac{1}{2}} = \frac{u_{i,j} - u_{i,j-1}}{\Delta r}, \qquad (\frac{\partial u}{\partial r})_{i,j-1} = \frac{u_{i,j+1} - u_{i,j-1}}{2\Delta r}$$

$$(\frac{\partial w}{\partial z})_{i,j} = \frac{1}{2\Delta z}(3w_{i,j} - 4w_{i-1,j} + w_{i-2,j})$$

$$w_{i+\frac{1}{2},j+1} = w_{i,j+1} + \frac{1}{4}(3w_{i,j+1} - 4w_{i-1,j+1} + w_{i-2,j+1})$$

$$w_{i-\frac{1}{2},j+1} = w_{i-1,j+1} + \frac{1}{4}(w_{i,j+1} - w_{i-2,j+1})$$

$$\phi_{i+\frac{1}{2},j+\frac{1}{2}} = \frac{1}{2}(\phi_{i+\frac{1}{2},j+1} + \phi_{i+\frac{1}{2},j}). \tag{2.9}$$

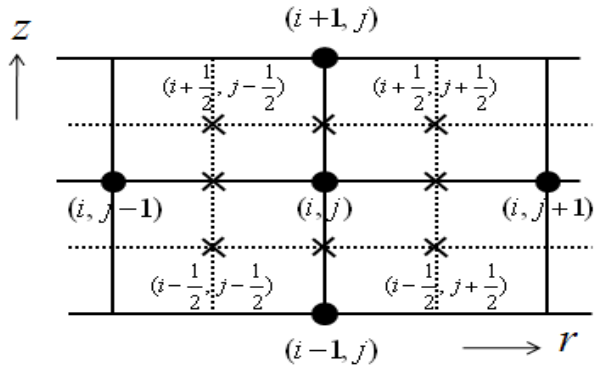

FIGURE 2. Finite volume mesh for a two-dimensional domain**.**

The subscript $\frac{1}{2}$ implies the value of the displacement at the boundary of the control surface (see Fig. 2). According to above relations at the adjacent locations the Eq. (2.8) is discretized as below

$$\begin{aligned}
&A_{11}u_{i+1,j} + A_{12}u_{i,j+1} + A_{13}u_{i,j-1} + A_{14}u_{i-1,j} + A_{15}u_{i,j} = 0,\\
&A_{21}u_{i,j+1} + A_{22}u_{i,j} + A_{23}u_{i,j-1} + A_{24}u_{i-1,j+1} + A_{25}u_{i-1,j} + A_{26}u_{i-1,j-1} + A_{27}u_{i-2,j+1} + A_{28}u_{i-2,j}\\
&+ A_{29}u_{i-2,j-1} + A_{30}w_{i+1,j} + A_{31}w_{i,j} + A_{32}w_{i-1,j} = K_i\alpha_i(1+\nu_i)r_j\Delta r[T_{i-\frac{1}{2}} - T_{i+\frac{1}{2}}]
\end{aligned} \tag{2.10}$$

The coefficients of Eq. (2.10) are the followings;

$$A_{11} = G_i r_j^{\,2}\frac{\Delta r}{\Delta z}, \qquad A_{12} = K_i(1-\nu_i)r_j r_{j+\frac{1}{2}}\frac{\Delta z}{\Delta r}, \quad A_{13} = K_i(1-\nu_i)r_j r_{j-\frac{1}{2}}\frac{\Delta z}{\Delta r}$$

$$A_{14} = G_i r_j^{\,2}\frac{\Delta r}{\Delta z}, \qquad A_{15} = K_i(1-\nu_i)(\Delta r\Delta z - r_j(r_{j+\frac{1}{2}} + r_{j-\frac{1}{2}})\frac{\Delta z}{\Delta r}) - 2G_i r_j^{\,2}\frac{\Delta r}{\Delta z},$$

$$A_{21} = \frac{1}{8}(G_i - K_i\nu_i)(5r_j + 4\Delta r), \qquad A_{22} = -\frac{1}{8}(G_i - K_i\nu_i)(10r_j + 8\Delta r),$$

$$A_{23} = \frac{1}{8}(G_i - K_i\nu_i)(5r_j + 4\Delta r), \qquad A_{24} = -(G_i - K_i\nu_i)r_j, \quad A_{25} = 2(G_i - K_i\nu_i)r_j,$$

$$A_{26} = -(G_i - K_i\nu_i)r_j, \qquad A_{27} = \frac{3}{8}(G_i - K_i\nu_i)r_j, \quad A_{28} = -\frac{1}{8}(G_i - K_i\nu_i)r_j,$$

$$A_{29} = \frac{3}{8}(G_i - K_i\nu_i)r_j, \qquad A_{30} = -K_i(1-\nu_i)r_j\frac{\Delta r}{\Delta z}, \qquad A_{31} = 2K_i(1-\nu_i)r_j\frac{\Delta r}{\Delta z},$$

$$A_{32} = -K_i(1-\nu_i)r_j\frac{\Delta r}{\Delta z}.$$

The stability properties to the scheme were appeared in the paper [3].

3. RESULTS AND DISCUSSION

For the temperature distribution profile and the thermoelastic characteristics the mechanical and thermal properties shown in Table I are used for each layer.

Table I. Mechanical and thermal properties for analyzing thermoelastic characteristics.

Material/Property	Elastic module (GPa)	Poisson's ratio	Thermal expansion coefficient (10^{-6}/°C)	Thermal conductivity (W/m-°C)
Top coat (204 C-NS: porous microstructure)	50	0.315	11.5	1.5
Top coat* (204 NS: dense Microstructure)	100	0.2	9.5 (20–1300 °C)	2.0
Bond coating (AMDRY 995C)	200	0.3	14	11
Substrate (NIMONIC 263)	221	0.3	11.1 (20–100 °C)	11.7

* Properties of top coat prepared using an air plasma spray with METCO 204 NS-G powder

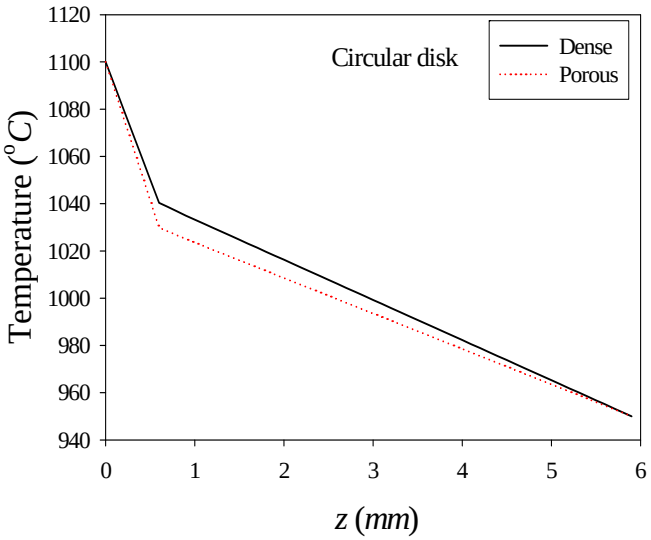

FIGURE 3. Temperature distribution profiles under the symmetric temperature distribution of 1100–950 °C.

According to the process developed in section 2.1 the temperature distribution profile of TBC model is obtained and displayed in Fig. 3. METECO 204NS and METCO 204C-NS feature a low thermal conductivity, which is presented at the top coat of TBC system. Metal concentration increases along the longitudinal direction and the rate of temperature decrease thus is getting slower. At the top coat of the porous TBC model the rate of temperature decrease is larger than of the dense TBC model and lower temperature distribution profiles appears overall the porous TBC model. The result demonstrates that the mathematical approach is reliable and reasonable.

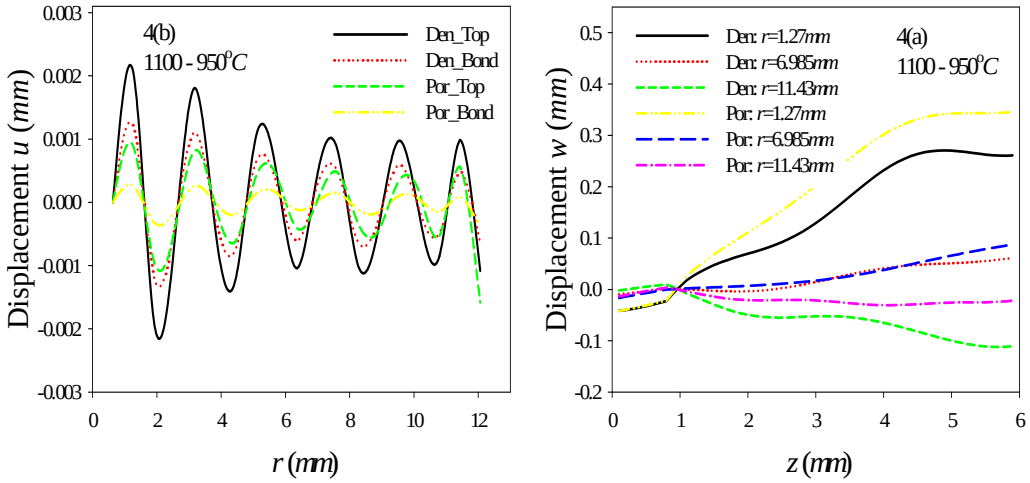

FIGURE 4. Displacements of the TBC model under the symmetric temperature distribution of 1100–950 °C: (a) longitudinal displacement (w) and (b) radial displacement (u).

The finite volume model developed in section 2.3 applied with the step size 12.7/20 and 0.1, respectively, for the radius r and longitude z to obtain the numerical solutions. Fig. 4 shows the displacement distribution profiles. The longitudinal displacements for some chosen values $r = 1.27$, 6.985, and 11.43 mm are shown in Fig. 4(a) and radial displacements shown in Fig. 4(b) at both the top and bond coats, respectively, depending on microstructure. For the values $r = 1.27$ and 6.985 mm the TBC model extends to the negative direction at the top and bond coats, and positive direction at the substrate. Larger extension turns up over the porous TBC model. For the value $r = 11.43$mm the extension of the dense TBC model develops to the positive direction at the top and bond coats, and negative direction at the substrate, whereas the porous extends to the negative direction only over the domain. The properties of the porous TBC model are presented well when the radius $r = 1.27$ and 6.985mm, that is the longitudinal displacement of the porous TBC is larger than of the dense TBC. On the other hand, the radial displacement shows a different phase from the longitudinal displacement. In comparison with the dense TBC model both the top and bond coats appear smaller displacement over the porous TBC model. The both top and bond coats progress along the radius with a fluctuation, which cause a failure mechanism such as a delamination.

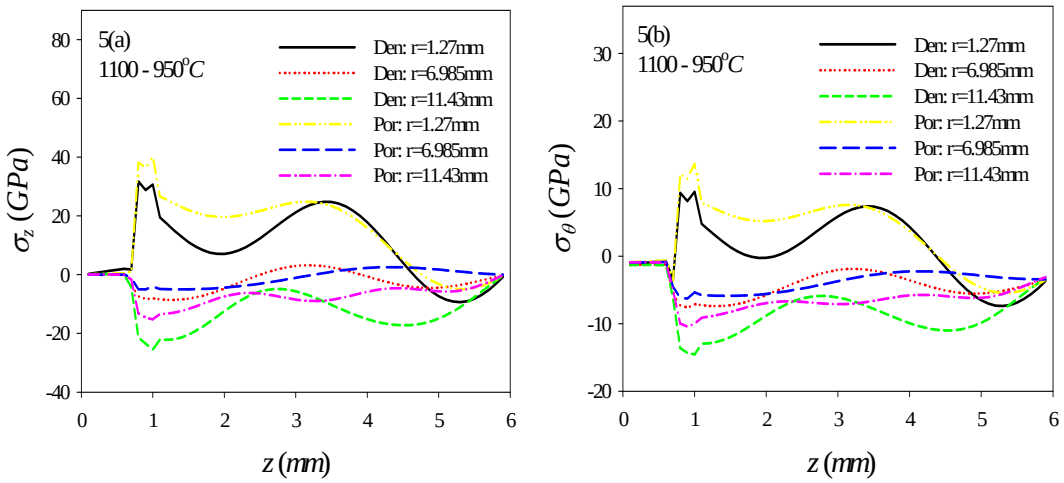

FIGURE 5. Stresses in the TBC model under the symmetric temperature distribution of 1100–950 °C: (a) longitudinal stress and (b) circumferential stress.

Fig. 5 exhibits the longitudinal and circumferential stresses some chosen values $r = 1.27$, 6.985, and 11.43 mm. At the $r = 1.27$ mm the interface between the top and bond coats of the porous TBC model is under the influence of the largest longitudinal tensile stress, while the largest compressive longitudinal stress takes place at the interface between the bond coat and the substrate of the dense TBC model when the radius is 11.43 mm (see Fig. 5(a)). The dense TBC model, near the center, is affected by larger longitudinal tensile stress at the interface between the top coat and bond coat, but, near the boundary larger longitudinal compressive stress occurs at the interface between the bond coat and the substrate. At the substrate of each TBC model an undulation develops for the longitudinal stress. The circumferential stress is shown in Fig. 5(b). Similar behaviors display to the longitudinal stress.

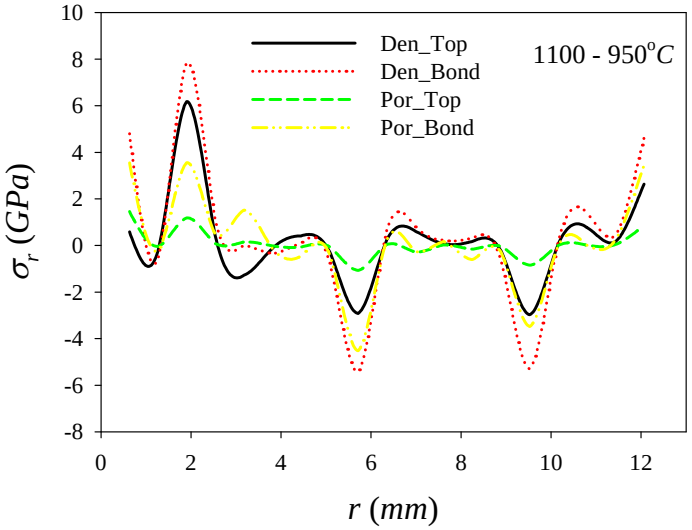

FIGURE 6. Radial stress in the TBC model under the symmetric temperature distribution of

1100–950 °C.

The radial stresses at the top and bond coats are presented in Fig. 6. The fluctuation carrying the largest magnitude appears at the bond coat of the dense TBC model, whereas the smallest undulation develops at the top coat of the porous TBC model. At the boundary of the domain the largest radial tensile occurs at the bond coat of the dense TBC model and the radial stress of the dense TBC model is larger than of the porous TBC model, which implies that the risk of failure mechanism is higher in the dense TBC.

4. CONCLUSION

The thermoelastic characteristics of the porous and dense TBC models have been investigated and compared with each other. In the positive longitudinal extension the porous TBC model displayed larger displacement, while radial displacement progressed with larger magnitude over the dense TBC model. Near the boundary larger longitudinal compressive stress developed over the porous TBC model, which diminishes the risk of failure mechanisms. The circumferential stress presented similar behaviors to the longitudinal stress. Overall, since the radial stress fluctuated with smaller magnitude in the porous TBC model, the thermal stability of TBC can be improved by controlling the microstructure at the top coat. In other words, the failure mechanisms can be reduced and the lifetime can be extended.

ACKNOWLEDGMENT

[1]This research was supported by Basic Science Research Program through the National Research Foundation of Korea (NRF) funded by the Ministry of Education, Science and Technology (2010-0024178). [1]This research is financially supported by Changwon National University in 2009-2010. [2,3]This work was supported by the Power Generation & Electricity Delivery of the Korea Institute of Energy Technology Evaluation and Planning (KETEP) grants funded by the Korea government Ministry of Knowledge Economy (R-2007-1-003-02 & 2009T100200025).

REFERENCES

[1] F. Cernuschi, P. Bison, and A. Moscatelli, Microstructural characterization of porous thermal barrier coatings by laser flash technique 57 (2009), 3460-3471, Acta Materials

[2] K.D. Harris, D. Vick, E.J. Gonzalez, T. Smy, K. Robbie, and M.J. Brett, Porous thin films for thermal barrier coatings 138 (2001),185-191, Surface and Coatings Technology

[3] M. Tadi, Finite Volume Mehod for 2D Elastic Wave Prooagation, 94 (2004),1500-1509, Bulletin of the Seismological Society of America,

[4] N. Zotov, M. Bartsch, L. Chernova, D.A. Schmidt, M. Havenith**,** and G. Eggeler, Effects of annealing on the microstructure and the mechanical properties of EB-PVD thermal barrier coatings, 15 (2010), 452-464, Surface and Coatings Technology

[5] P. Roy, G. Bertrand, and C. Coddet, Spray drying and sintering of zirconia based hollow powders 157 (2005), 20-26, Powder Technol.

[6] S.-I. Jung, J.-H. Kim, J.-H. Lee, Y.-G. Jung, U. Paik, and K.-S. Lee, Microstructure and mechanical properties of zirconia-based thermal barrier coatings with starting powder morphology 204 (2009), 802-806, Surface and Coatings Technology